A computational study of the properties of Pd, Cu and Zn surfaces

Lara Kabalan[1], Igor Kowalec[1], C. Richard A. Catlow[1,2,3] and Andrew J. Logsdail[1,*]

[1] Cardiff Catalysis Institute, School of Chemistry, Cardiff University, Park Place, Cardiff, CF10 3AT, Wales, UK

[2] Department of Chemistry, University College London, 20 Gordon Street, London, WC1E 6BT, UK

[3] UK Catalysis Hub, Research Complex at Harwell, Rutherford Appleton Laboratory, Didcot, OX11 OFA, UK

Correspondence address: LogsdailA@cardiff.ac.uk

Abstract: We report a detailed Density Functional Theory (DFT) based investigation of the structure and stability of bulk and surface structures for the Group 10-12 elements Pd, Cu and Zn, considering the effect of the choice of exchange-correlation density functionals and computation parameters. For the initial bulk structures, the lattice parameter and cohesive energy are calculated, which are then augmented by calculation of surface energies and work functions for the lower-index surfaces. Of the 22 density functionals considered, we highlight the mBEEF density functional as providing the best overall agreement with experimental data. The optimal density functional choice is applied to the study of higher index surfaces for the three metals, and Wulff constructions performed for nanoparticles with a radius of 11nm, commensurate with nanoparticle sizes commonly employed in catalytic chemistry. For Pd and Cu, the low-index (111) facet is dominant in the constructed nanoparticles, covering ~50% of the surface, with (100) facets covering a further 10 to 25%; however, non-negligible coverage from higher index (332), (332) and (210) facets are also observed for Pd, and (322), (221) and (210) surfaces are observed for Cu. In contrast, only the (0001) and (10-10) facets are observed for Zn. Overall, our results highlight the need for carefully validation of computational settings before performing extensive density functional theory investigations of surface properties and nanoparticle structures of metals.

Introduction

Computer simulation and computer-assisted design provides a powerful approach for understanding and optimizing functional materials [1,2]; and detailed knowledge of surface properties is necessary in understanding the applied chemistry, including catalytic behaviour, of materials. A particularly important quantity is the surface energy [3], which is crucial in determining surface structure, including for nanoparticulate systems with high surface areas and non-crystalline cores. In experiment, the surface energy is measured from a set of liquid/solid contact angles when liquids are brought in to contact with the solid of interest. Materials with a high surface energy show good wetting and a low contact angle, whilst low surface energy materials exhibit poor wetting and a higher contact angle.

Due to the specific nature of surface interactions, reactivity and solubilities, it is not possible to choose a universal set of liquids for use in testing solid surfaces [3,4,5,6]. As a result, such measurements are difficult and provide an incentive for the development of reliable computational modelling procedures. The surface energy can be calculated through the use of interatomic potentials, or as in most recent work, quantum mechanical methods, especially density functional theory (DFT) [7,8,9,10,11,12]. Such is the ease and availability of high-throughput density functional theory, Vitos *et al*. have recently created a database of surface energies computed for the low index surfaces of 60 metals, computed using a full charge density (FCD) approach [9] that provides efficient and accurate energetics. In this approach, the Hartree and exchange correlation part of the energy functionals are calculated from the charge density, using LDA or GGA functionals, while the kinetic energy is calculated from the Kohn-Sham kinetic energy, using full potential linear muffin-tin orbitals (LMTO) with the atomic-sphere approximation. The results compare well with other computational investigations that used density functionals (DF) for surface energy and the work function [9]. Cramer *et al.*[13] reviewed the accuracy of GGA, meta-GGA, hybrid, hybrid meta- and range-separated hybrid DFs for the simulation of transition metals, discussing the implications for bulk band structures, structural and spectroscopic properties; and reactivity. Tran *et al.* [11] also published a database of surface energy calculations for 70 elements,

with properties calculated employing the GGA approach of Perdew, Burke and Ernzerof (PBE) [14] and compared broadly to computation and experiment. Patra *et al.*[15] studied the (111), (110) and (100) surfaces of metals from Groups 9 to 11 of the periodic table (Pd, Pt, Cu, Ag, Ru, Rh, and Au), as well as the main group metal Al, which are all face centered cubic (FCC) metals, using six various DFs: LDA, PBE, PBEsol, SCAN, SCAN+rVV10 and RPA. The investigators concluded that the SCAN functional complemented by non-local van der Waals (vdW) corrections from the revised Vydrov–Van Voorhis 2010 (rVV10) DF, SCAN+rVV10 [16], gave the most accurate agreement with experiment for both surface energies and mean work functions.

Despite these detailed computational studies of metal surfaces, there remains a need for a systematic and uniform study of the importance of choice of functional and simulation parameters when modelling both low and high index surfaces of densely packed FCC and HCP metals, as commonly applied to catalytic chemistry, in order to identify how the choice of DF and numerical settings can impact the validity of these simulations. In the context of catalysis, high index surfaces are particularly important as they can exhibit high activity [17] when used as catalysts in fuel cells, petrochemical reforming and automotive catalytic converters, due to the higher density of low coordinated sites; and metal catalysts with high-index planes can display enhanced activity relative to close-packed low-index facets such as (111), (110) and (100) planes, such as for Pt [18]. High-index facets and high surface-energy nanocrystals also have wider applications such as in drug treatment, sensing and optics [19], stimulating further attention for both simulation and experiment. Quan *et al.* [20] studied high index surfaces for Pd and Pt metals and found that (730) and (411) facets of Pt show improved reactivity towards acid and ethanol oxidation, while the (720) facet offers improved rates for oxygen reduction reaction compared to low index surfaces (100) and (111). The Pd (730) facet also shows improved reaction yield when used as a catalyst for electro-oxidation of formic acid and in the Suzuki coupling reaction [21].

In this work, we address two key aspects of computational modelling of metal surfaces, namely the choice of simulation settings and functionals and their use in investigating the properties of high-index surfaces. We present a thorough analysis of the parameters needed for accurate bulk and surface calculations, including for high index surfaces, with specific focus on late-transition FCC (Pd. Cu) and HCP (Zn) metals, representing elements from Group 10, 11 and 12 of the periodic table. In the following section we summarize our methodology; subsequently, results for bulk calculations with 22 exchange-correlation DFs are compared to experimental lattice parameters and cohesive energies, and the best performing DFs are then used to calculate surface energies and work functions for relevant low- and high-index surfaces. We discuss the effect of variation in calculation parameters for surfaces, such as slab thickness, in order to highlight the attention to detail necessary when configuring such simulations. Finally, we present and discuss Wulff constructions of nanoparticles formed with the differing choices of DF, in order to highlight the impact of such approximations.

Methodology

i. Density Functional Theory (DFT) simulations

All calculations have been performed with the "Fritz Haber Institute ab initio molecular simulations" (FHI-aims) all-electron full potential software package [22], coupled with the LibXC DF library [23], using the light basis set and a **k**-grid density of (0.018 x 2π) $Å^{-1}$ unless otherwise stated. The self-consistent field (SCF) cycle was deemed converged when the changes in total energy and density were less than $1e^{-6}$ eV and $1e^{-6}$ e a_0^3, respectively. Throughout, a spin-paired configuration has been used with scalar relativity included via the atomic zero order regular approximation (ZORA) [24]. The exchange-correlation density functionals considered in this study are presented in Table 1. To check the effect of non-local van der Waals corrections, the Tkatchenko-Scheffler (TS) [25] and the non-local many-body dispersion (MBD-NL) [26] corrections were applied with PBE; the TS correction was also tested with PBE0.

Table 1. List of exchange-correlation density functionals considered in this study.

Approximation	Density Functionals
GGA	PBE [14], PBEsol [27], revPBE [28], RPBE [29], PBEint [30], PW91 [31], B97-D [32], R48PBE [33], HCTH-407 [34], BLYP [35]
meta-GGA	SCAN [36], revSCAN [37], TPSS [38], TPSSloc [39], revTPSS [40], mBEEF [41]
Hybrid-GGA	PBE0 [42], B3LYP [43], HSE06 [44]

ii. Bulk and surface models

Optimal lattice parameters for bulk Pd, Cu and Zn were obtained with equation-of-state calculations on the primitive cell [45]. Using optimal lattice parameters, surface slab models have been created in the Atomic Simulation Environment (ASE) Python package [46]. For Pd and Cu, which are FCC, the (111), (100), (110) surface facets were constructed; for Zn, which is HCP, the (0001) and (10-10) facets have been constructed (Figure S1-S5, Supporting Information (SI)). Unless otherwise stated, the slabs models have 7 atomic layers in the *z*-direction perpendicular to the surface, and a converged 20 Å

vacuum has been added in the *z*-direction to prevent interaction between periodic surfaces. The top 4 atomic layers are unconstrained during geometry optimization, with constraints applied to the remaining 3 layers, unless otherwise stated. The Broyden-Fletcher Goldfarb-Shanno (BFGS) algorithm is employed for geometry optimizations [47], with a force convergence of $1e^{-2}$ eV/Å. A dipole correction is applied in the *z*-direction to eliminate any electrostatic effects that could result from an asymmetric slab relaxation.

iii. Energy analysis

The cohesive energy of the bulk material, E_{coh}, is defined as:

$$E_{\mathrm{coh}} = \frac{E_{\mathrm{bulk}}}{n} - E_{\mathrm{atom}} \tag{1}$$

where E_{bulk} is the energy of bulk unit cell containing n atoms, and E_{atom} is the energy of the gas-phase metal atom. The spin on the gas-phase atom was set to zero for Pd and Zn, as they have a d^{10} and $d^{10}s^2$ valence electron configuration, respectively, while it was set to one for Cu which has a $d^{10}s^1$ configuration.

The surface energy, E_{surf}, is calculated as a combination of the surface cleavage energy, E_{cleav} , and the subsequent stabilizing relaxation energy, E_{relax}, which are obtained as [48]:

$$E_{\mathrm{cleav}} = \frac{E_{\mathrm{slab}}^{\mathrm{unrelax}} - NE_{\mathrm{bulk}}}{2\mathrm{A}_{\mathrm{slab}}} \tag{2}$$

$$E_{\mathrm{relax}} = \frac{E_{\mathrm{slab}}^{\mathrm{relax}} - E_{\mathrm{slab}}^{\mathrm{unrelax}}}{\mathrm{A}_{\mathrm{slab}}} \tag{3}$$

$$E_{\mathrm{surf}} = E_{\mathrm{cleav}} + E_{\mathrm{relax}} \tag{4}$$

where N is the number of bulk units in the slab model, and A_{slab} is surface area of the model. A factor of two is included in the denominator of E_{cleav} as there are surfaces on the top and bottom of the cleaved slab, where relaxation is one-sided only.

iv. Work function:

The work function (Φ) of a material is defined as the minimum energy required to move an electron from the surface to a far distance (i.e. vacuum). The work function is given by [49]:

$$\Phi = V_{\text{vac}} - \varepsilon_{\text{Fermi}} \quad (5)$$

Where V_{vac} is the maximum of the electrostatic potential at the centre of vacuum, and $\varepsilon_{\text{Fermi}}$ is the Fermi energy. The work function depends on the crystallographic facet [50].

v. Wulff construction:

The Wulff construction of nanoparticles has been performed using the Wulffpack Python package [51]. The morphology of equilibrium crystals is obtained, according to the Gibbs thermodynamic principle, by minimizing the total surface free energy (here approximated by electronic energy) associated to the crystal-medium interface.

Results

i. Bulk lattice parameters and cohesive energy

The calculated lattice parameters (a_0) and cohesive energy (E_{coh}) using each DF, as well as the percentage difference with respect to room temperature experiment [52], are reported in Table S1-S3 of the SI. Thermal corrections to the experimental data are not explicitly considered in the analysis here, having been recognized in previous work to only marginally decrease mean percentage absolute errors (MPAE) for geometric distances and cohesive energies, by 0.04 % and 0.2 %, respectively.[53,54]

In order to assemble the results for each DF for collective analysis here, the MPAE is calculated for each XC and material, considering both a_0 and E_{coh}, with respect to the experiment values:

$$MPAE = \frac{1}{Y}\left[\sum_{i=1}^{Y}\left(\frac{y_i - x_i}{y_i}\right) \times 100\right] \quad (5)$$

where y_i is the calculated value of the observable and x_i is the corresponding experimental result. Y is the number of observables studied, and therefore is equal to two for FCC Pd and Cu, reflecting the lattice parameters a_0 and E_{coh}, and three for HCP, due to the additional lattice parameter c_0. The calculated and average MPAE for each DF are plotted in Figure 1, with data presented in Table 2.

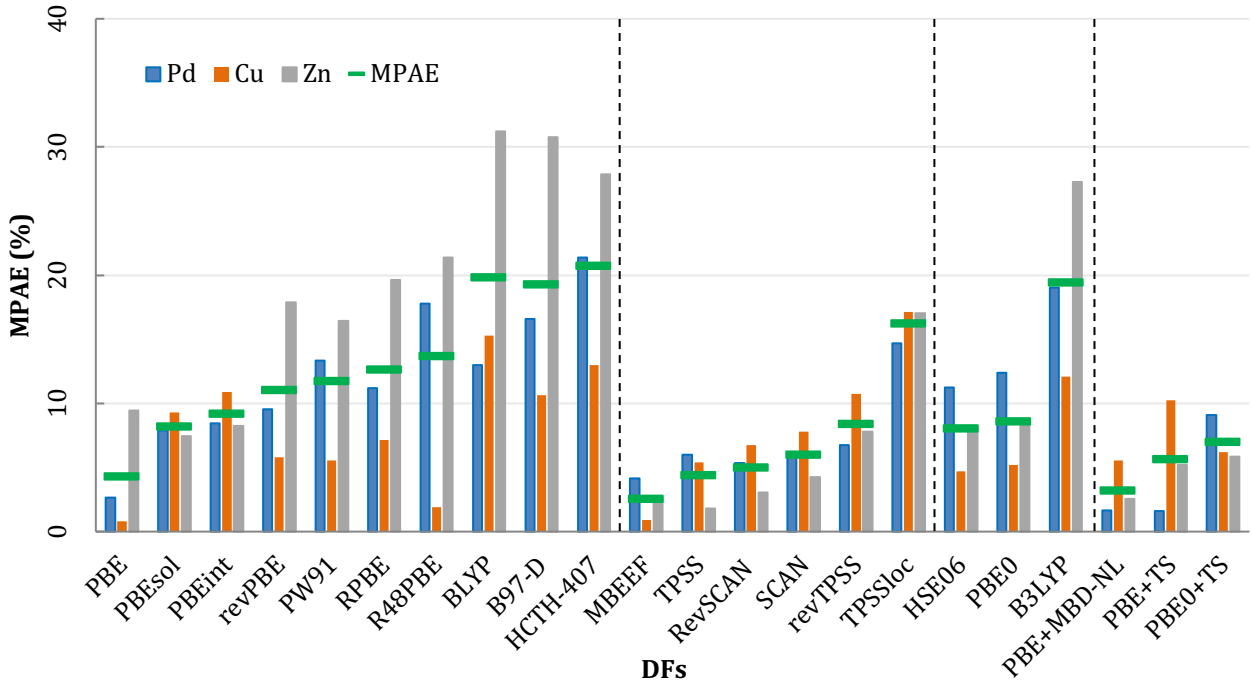

Figure 1. The MPAE of each density functional as calculated for bulk Pd, Cu and Zn.

Table 2: MPAE for each density functional when applied to calculate equilibrium bulk structures, and associated cohesive energy, of Pd, Cu and Zn. The results are ordered descending, from best to worst, with respect to the MPAE within each DF approximation sub-category (GGA, meta-GGA, hybrid).

DF		**MPAE**			
		Pd	**Cu**	**Zn**	**Mean**
GGA	PBE (+TS) (+MBD-NL)	2.65 (1.61) (1.67)	0.80 (10.22) (5.54)	9.46 (5.17) (2.53)	4.30 (5.67) (3.25)
	PBEsol	7.91	9.29	7.42	8.21
	PBEint	8.47	10.90	8.25	9.21
	revPBE	9.53	5.82	17.89	11.08
	PW91	13.31	5.54	16.43	11.76
	RPBE	11.17	7.14	19.46	12.59
	R48PBE	17.78	1.89	21.38	13.68
	B97-D	16.58	10.62	30.78	19.33
	BLYP	13.01	15.30	31.23	19.85
	HCTH-407	21.36	12.98	27.86	20.73
Meta-GGA	mBEEF	4.14	0.93	2.60	2.56
	TPSS	6.01	5.41	1.78	4.40
	revSCAN	5.37	6.72	3.04	5.04
	SCAN	6.01	7.79	4.27	6.02
	revTPSS	6.76	10.76	7.79	8.44
	TPSSloc	14.66	17.11	17.03	16.27
Hybrid	HSE06	11.23	4.69	8.23	8.05
	PBE0 (+TS)	12.36 (9.07)	5.21 (6.19)	8.24 (5.84)	8.60 (7.03)
	B3LYP	19.04	12.10	27.26	19.47

For all the exchange-correlation DFs considered, the error in E_{coh} is generally higher than the error for a_0 and c_0, especially in the case of Zn. The poor accuracy of E_{coh} for Zn has been observed previously by Lejaeghere *et al.* [53], who highlighted a difference of 20 % when using PBE; similar observations are reported by Janthon *et al.* [54], who reported a difference of 29 %. In an attempt to address the discrepancies highlighted, Lejaeghere *et al*. [53] applied zero point and finite temperature phonon corrections to the experimental data; however, these corrections result in only marginal improvements against experiment, thus failing to resolve the significant error. For PBE, the addition of a vdW correction (PBE+TS) provides better agreement between the calculated lattice parameters and experiment; however, the resulting cohesive energies are much greater than experiment, especially for Cu (Calculated: 4.14 eV, Experiment: 3.49 eV). Similar results are observed for the PBE0 functional with TS included, which highlights the complexity in identifying DFs that can accurately model structure *and* energetics for multiple systems.

Of the DFs considered, BLYP, B97-D, HCTH-407, B3LYP, R48PBE and RPBE functionals have a high MPAE for Zn (31.23, 30.78, 27.86, 27.26, 21.38, and 19.46% respectively), which contributes strongly to an overall high mean MPAE. PBEsol, HSE06, revTPSS and PBEint have an intermediate MPAE, in the range from 6 to 10%, while PBE, PBE+TS, PBE+MBD-NL, TPSS, SCAN, revSCAN, and mBEEF have an MPAE of < 6%. The lowest MPAE is obtained for mBEEF, at 2.56%. The accuracy of mBEEF arises from a combination of machine learning with a Bayesian concept to generalize the fitting procedure for a broad range of material properties [41], providing generally accurate cohesive energies and lattice parameters.

ii. Surface energy

DFs with an MPAE < 6% for bulk structure and energetics have been taken forward for surface energy studies; these include the PBE, PBE+TS, PBE+MBD-NL, TPSS, SCAN, revSCAN and mBEEF exchange-correlation DFs.

***a.* Quantum size effect**

To model surfaces in a periodic framework, slab representations of the target system are constructed, such that the system is continuous in the *x*- and *y*- directions but finite in the *z*-direction. The discretization of the model in the *z*-direction can create a quantum size effect (QSE) for thin models, manifested by oscillations of the energy when the slab thickness changes, which creates a need to converge carefully the model thickness to ensure chemical accuracy. Previously, Schulte [55] demonstrated the QSE for a jellium slab model with the oscillation of the work function calculated depending on the slab thickness; similarly, Da Silva *et al.* [2] demonstrated that QSE for Cu(111) with varying slab thicknesses, with convergence of surface energy achieved by including seven atomic layers in the *z*-direction and applying very dense **k**-grid sampling in the *x*- and *y*-directions (32x32x1).

Figure 2 presents our results using the PBE DF to calculate surface energies as function of slab depth. We considered the Pd (111), (100) and (110) facets, and oscillations in the surface energy are observed with varying numbers of layers; the oscillations are most pronounced for sparser **k**-grid densities of (0.039 x 2π) $Å^{-1}$, with variation of 0.06 J/m^2 between 9- and 10-layer slab (111) models. The oscillations decrease with increasing **k**-grid density, and are reduced across all facets for a **k**-grid density of (0.018 x 2π) $Å^{-1}$; however, even with a dense **k**-grid sampling of one **k**-point per (0.011 x 2π) $Å^{-1}$, oscillations of 0.01 J/m^2 are present for the models of the (110) facet. Structural analysis shows these minor fluctuations are due to the crystallographic cleaving creating a 'cranulation', which causes the electronic structure to alternate between even and odd layer numbers, resulting in changes in the electrostatic potentials and therefore the onsite energies [56]. An equivalent analysis for Cu (111), (100), and (110) facets, and Zn (0001) and (10-10) facets, shows similar oscillations in the surface energy

are reduced when increasing the **k**-grid density (Figures S6 and S7, SI). Comparing all systems, a slab thickness of seven layers, with a **k**-grid density of one **k**-point per (0.018 x 2π) $Å^{-1}$, is deemed necessary to minimise the QSE in our slab calculations.

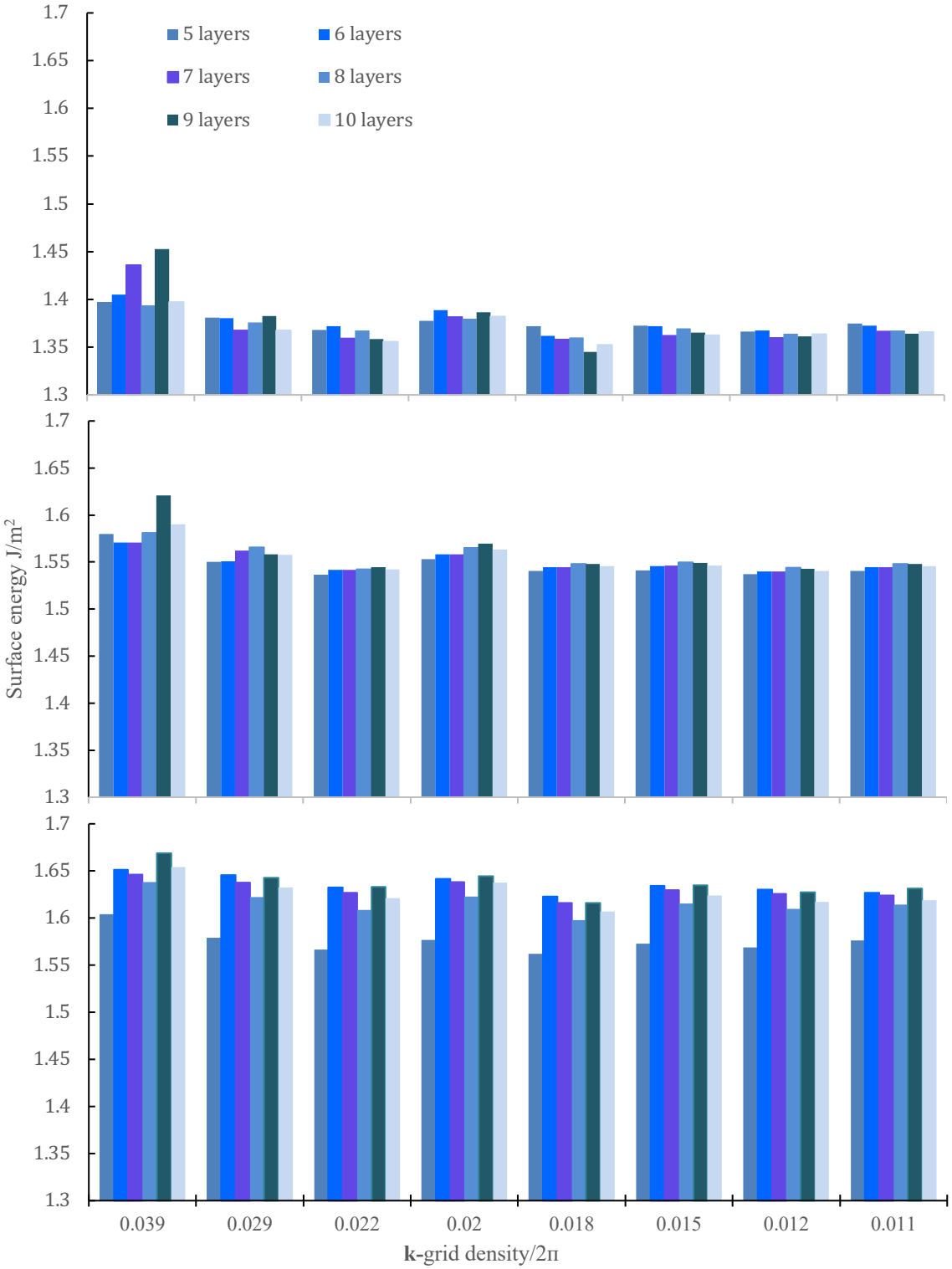

*Figure 2: The surface energy (Jm^{-2}) for Pd (111), (100) and (110) facets, given in the top, middle and bottom graphs, respectively, as function of **k**-grid density ($Å^{-1}$) in the x- and y-directions. A key is given to show how many layers (5-10) were considered in the respective models.*

b. Exchange-correlation density functional

The surface energies for Pd, as calculated with the prescribed range of exchange-correlation DFs and verified numerical settings from Section *III.ii.a*, are presented in Table 3; results from previous computational and experimental studies are also given, with the experimental data of Tyson *et al.* reported at 0 K and at the melting temperature of 1591K.

Table 3: The surface energy (J/m^2) of Pd (111), (100) and (110) surface facets, as calculated with different density functionals. Results from the present study are given in bold.

Facet / DF	(111)	(100)	(110)	(111)/(100)	(111)/(110)
PBE	**1.36**	**1.54**	**1.60**	**0.86**	**0.85**
Da silva *et al.*[2]	1.36				
Patra *et al.*[15]	1.36	1.79	1.61	0.76	0.84
Tran *et al.*[11]	1.36	1.52	1.57	0.89	0.86
Singh-Miller *et al.* [49]	1.31	1.49	1.55	0.88	0.84
Lin *et al.* [57]	1.33	1.51	1.60	0.88	0.83
PBE+TS	**1.52**	**1.64**	**1.74**	**0.92**	**0.87**
PBE+MBD-NL	**1.64**	**1.72**	**1.80**	**0.95**	**0.91**
TPSS	**1.67**	**1.82**	**1.95**	**0.92**	**0.86**
SCAN	**1.67**	**1.80**	**1.88**	**0.92**	**0.89**
Patra *et al.*[15]	1.54	2.08	1.83	0.74	0.84
revSCAN	**1.75**	**1.90**	**1.97**	**0.92**	**0.89**
mBEEF	**1.32**	**1.50**	**1.58**	**0.88**	**0.83**
Experiment, Tyson *et al.*:					
T = 0 K [58]	1.63			-	-
T = 1828 K [3]	1.74			-	-

For all the exchange-correlation DFs considered here, the surface energy of the (111) facet is lower than the (100) and (110) surfaces, agreeing with other theoretical work[11,49]. The agreement of our PBE results with previous simulations is good (± 0.05 J/m^2) with the exception of the investigations of Patra *et al.* [15] who report the (100) surface energy to be greater than (110), contrary to all other studies. The addition of the Tkatchenko-Scheffler vdW correction to PBE (PBE+TS) increases the surface energies for the (111), (100) and (100) facets by 0.16, 0.1 and 0.14 J/m^2, respectively, bringing

the energies closer to the experimental values. The same increases in surface energy are observed for PBE+MBD-NL, relative to PBE, with increases of 0.28, 0.18 and 0.20 J/m^2, for the (111), (100) and (110) surfaces, respectively. For the meta-GGA DFs, TPSS and SCAN give almost identical surface energies for (111) and (100) facets, which are similar to experimental results, whilst the surface energy of the (110) facet is slightly greater with TPSS. revSCAN gives larger surface energies compared to SCAN and is further from the experimental measurements; in contrast, mBEEF gives the lowest surface energies of 1.32, 1.50 and 1.58 J/m^2 for the (111), (100) and (110) facets, respectively.

Direct comparison for each Pd surface facet with experiment is not straightforward, as experimental surface energies are averaged over the various crystal facets (1.63 J/m^2 at 0 K, and 1.74 J/m^2 at the 1828 K [3,58]); however, broad comparison of each DF with experiment can be made. Comparing our average results for each DF with experiment leads to the conclusions, firstly, that PBE and mBEEF underestimate the surface energies of Pd by a small amount (averages of 1.50 and 1.46 J/m^2, respectively); secondly, that PBE+TS and PBE+MBD-NL compare well with experiment (averages of 1.63 and 1.72 J/m^2, respectively); and finally, that all other DFs overestimate the surface energy of Pd.

The ratio of surface energies is an alternative metric of DF accuracy. Such ratios are important as they determine the equilibrium nanoparticle shape and the dominant facets; for instance, the smaller the ratio of (111)/(100) surface energies, the more the (111) facet dominates the nanoparticle surface. Recently, Chen *et al.* [59] reported experimental measurements for Pd of 0.77±0.02 for the (111)/(100) surface energy ratio, obtaining the equilibrium nanoparticle shape by annealing at 450 °C. From our calculations, closest agreement with experiment is for the PBE (0.86) and mBEEF (0.88) DFs; all other approaches predict a ratio > 0.92. We also present in Table 3 the calculated (111)/(110) ratio for Pd, and note that the trends are inconsistent compared to the (111)/(100) ratio, with the lowest ratio obtained with mBEEF (0.83) and the highest with PBE+MBD-NL (0.91).

The surface energies calculated for Cu (111), (100) and (110) facets are reported in Table 4, where they are compared with previous computational and experimental work. It is noted for Cu that Tyson *et al.* report experimental surface energies at T = 0 K of 1.79 J/m^2 and then 1.57 J/m^2 at the melting temperature (T = 1357 K), *i.e.* a decrease in the surface energy with increasing temperature, in contrast to results for Pd (Table 3).

Table 4: The surface energy (J/m^2) of Cu, (111), (100) and (110) surface facets, as calculated with different density functionals. Results from the present study are given in bold.

Facet / DF	(111)	(100)	(110)	(111)/(100)	(111)/(100)
PBE	**1.37**	**1.51**	**1.58**	**0.91**	**0.87**
Da silva[2] *et al.*	1.41				
Da silva[60] *et al.*	1.32	1.48	1.59	0.76	0.83
Patra *et al.*[15]	1.36	1.79	1.61	0.91	0.84
Tran *et al.*[11]	1.34	1.47	1.56	0.90	0.86
PBE+TS	**2.57**	**2.72**	**2.77**	**0.94**	**0.93**
PBE+MBD-NL	**1.80**	**1.93**	**1.99**	**0.93**	**0.90**
TPSS	**1.60**	**1.77**	**1.93**	**0.90**	**0.83**
SCAN	**1.58**	**1.78**	**1.90**	**0.93**	**0.83**
Patra *et al.*[15]	1.49	1.71	1.84	0.87	0.80
revSCAN	**1.75**	**1.93**	**2.02**	**0.90**	**0.67**
mBEEF	**1.43**	**1.56**	**1.63**	**0.92**	**0.88**
Experiment, Tyson *et al.*:					
T = 0 K [58]	1.79			-	-
T = 1357 K [3]	1.57			-	-

For the GGA functionals, again PBE provides low surface energies, with 1.37, 1.51 and 1.58 J/m^2 for the (111), (100) and (110) facets; these are marginally below the experimental values, also. Inclusion of van der Waals correlation corrections, using the TS approach (PBE+TS), results in seemingly poor agreement with experiment, as the surface energies increase dramatically to 2.57, 2.72 and 2.77 J/m^2 for the (111), (100) and (110) facets, respectively. For the meta-GGA DFs, SCAN and TPSS again give very similar results, as observed for Pd; mBEEF also gives relatively low surface energies, compared to contemporary meta-GGA methods, of 1.43, 1.56 and 1.63 J/m^2 for (111), (100)

and (110) facets, respectively; these are again similar to the PBE results. As a consequence, the average surface energy for the three facets obtained by PBE (1.49 J/m^2) and mBEEF (1.54 J/m^2) are similar, again being lower than the experimental results, while TPSS and SCAN give results closer to experiment. The average result for PBE+TS (2.68 J/m^2) is anomalously large compared to experiment, and further investigation is warranted to understand the cause of this result.

Previous measurement of the ratios for (111)/(100) surface energies for Cu facets are absent from the current literature; in the present work, the ratio of (111) to (100) surface energies is calculated to range from 0.88 (PBEsol) to 0.94 (PBE+TS). The (111)/(110) ratio has a similar range, from 0.82 to 0.94.

Table 5 reports the surface energies calculated for the (0001) and (10-10) facets of HCP Zn, together with computational work by Tran *et al.* [11] and the experimental data of Tyson *et al* [3,58].

Table 5: The surface energy (J/m^2) of Zn (0001) and (10-10) surface facets, as calculated with different density functionals. Results from the present study are given in bold.

Facet / DF	(0001)	(10-10)	(0001)/(10-10)
PBE	**0.32**	**0.97**	**0.33**
Tran *et al.*[11]	0.33	0.53	0.62
PBE+TS	**0.92**	**1.73**	**0.53**
PBE+MBD-NL	**0.49**	**1.22**	**0.40**
TPSS	**0.50**	**1.34**	**0.37**
SCAN	**0.44**	**1.19**	**0.37**
revSCAN	**0.06**	**1.30**	**0.04**
mBEEF	**0.24**	**1.17**	**0.20**
Experiment, Tyson *et al.*			
T = 0 K [3]	0.92	-	-
T =692 K [58]	0.99	-	-

The Zn surface energies presented in Table 5 span a wide range of energies. revSCAN and PBEsol give the lowest surface energies for the (0001) facet, of just 0.06 J/m^2 and 0.14 J/m^2 respectively, while PBE+TS gives the highest value of 0.92 J/m^2. All other DFs give surface energies

for the (0001) facet between 0.24 J/m^2 to 0.50 J/m^2, seemingly well below the experimental results; the results obtained for the PBE DF are noted, however, to be in excellent agreement with the previous computations of Tran *et al.* [11].

The surface energies calculated for the (10-10) facet are much larger than the (0001) facet, with the lowest value obtained for PBE (0.99 J/m^2) and a maximum for PBE+TS (1.73 J/m^2). Interestingly, the (10-10) surface energy calculated here with PBE is much larger than that reported by Tran *et al.*[11], which we attribute to differences in nearest neighbour distances; in their work, the nearest neighbor separations are smaller than the experimental values. Overall, the surface energies of the (0001) facet are much lower than the (10-10) facet, though values calculated for the latter are noticeably closer to the experimental results.

We conclude our study of Zn by tentatively calculating a ratio of (0001)/(10-10) facet energies for each DF. The span of ratios is large, with the smallest ratio observed for revSCAN (0.03), and the largest ratios observed being 0.40 and 0.53, with PBE-MBD-NL and PBE+TS, respectively. We note that the (0001)/(10-10) ratio is potentially misleading when the surface energy of (0001) is computed as being very low, such as for revSCAN, and future studies will further investigate the causes of these observations.

iii. Work function

We note that QSE has been detected also when calculating the work function of materials. As an example, for Pd(110) in our work, Φ calculated with PBE is equal to 5.39 or 5.75 when using a **k**-grid density of (0.039 x 2π) or (0.029 x 2π) Å^{-1}, respectively; this value is stable at 4.80 eV for a **k**-grid density of (0.02 x 2π) Å^{-1} and below. Given that we have identified the necessary computational parameters to minimize QSE in slab calculations, Φ is calculated herein for the optimized slab models, as considered when calculating surface energy (i.e. with the same numerical settings).

Values of the work function (Φ) for Pd, as calculated with each considered DF, are presented in Table 6. For all the DFs considered, the work functions decrease in line with surface energies, such

that Φ (111) > Φ (100) > Φ (110). For the (111) facet, the best match between calculation and experiment was obtained with TPSS, with a difference of 1.10 %; the greatest difference was 4.96 % with PBE+MBD-NL and mBEEF, which both under-estimate Φ (5.17 eV). For the (100) facet, SCAN and TPSS match well with experiment, with a difference of 1.51 %, while the largest difference is for mBEEF (5.85 %). The similarity between TPSS and SCAN for electronic properties is interesting, given their similarity also for energetics in Tables 3-5. Finally, for the (110) facet, PBE and mBEEF agree accurately with experiment, while SCAN gives the largest difference (7.50 %).

Table 6: The work function (eV) of Pd as calculated with each exchange-correlation DF, presented alongside previous computational and experimental results. Results from the current work are highlighted in bold, and the percentage difference (%) are given in parentheses relative to the experimental measurement of Fisher et al. [61] for the (111) facet, Küppers et al. [62] for the (100) facet, and Gay et al. [63] for the (110) facet.

DF \ Facet	(111)	(100)	(110)
PBE	**5.19** *(-4.60)*	**5.02** *(-5.28)*	**4.80** *(0.00)*
Da Silva *et al*.[2]	5.64		
Patra *et al.*[15]	5.32	5.12	4.95
Tran *et al.*[11]	5.20	5.13	4.62
Singh-Miller *et al*[49]	5.25	5.11	4.87
PBE+TS	**5.24** *(-3.67)*	**5.04** *(-4.91)*	**4.85** *(+1.04)*
PBE+MBD-NL	**5.17** *(-4.96)*	**5.04** *(-4.91)*	**4.77** *(-0.62)*
TPSS	**5.50** *(+1.10)*	**5.38** *(+1.51)*	**5.11** *(+6.46)*
SCAN	**5.51** *(+1.29)*	**5.38** *(+1.51)*	**5.16** *(+7.50)*
Patra *et al*.[15]	5.39	5.19	5.04
RevSCAN	**5.42** *(0.37)*	**5.03** *(-5.09)*	**4.82** *(+0.42)*
mBEEF	**5.17** *(-4.96)*	**4.99 (-5.85)**	**4.80 (0.00)**
Derry *et al.* [62]	5.67 ± 0.12	5.48 ± 0.23	5.07 ± 0.2
Fisher *et al.* [61]	5.44 ± 0.03	-	-
Küppers *et al.* [64]	-	5.3	-
Gay *et al.* [63]	-	-	4.8

The work function data for Cu are presented in Table 7 compared with other computational and experimental work. For the (111) facet, SCAN predicts a value of Φ that is very close to experiment (4.89 for 4.94 eV [65], respectively) with an difference of 1.01 %, followed by mBEEF with

a difference of 2.23 %, while PBE+MBD-NL give a large difference (4.71 eV, 4.66 %). For the (100) facet, TPSS gives the value of 4.59 eV reported experimentally [66], with mBEEF also performing well (4.53 eV, 1.31 %) while a larger deviation was obtained with PBE (4.44 eV, 3.27 %). For the (110) facet, the calculated Φ using TPSS is in good agreement with experiment (4.50 eV for 4.45 eV, respectively) [62] with a difference of 1.12 %, followed by PBE and mBEEF [4.35 eV (2.25 %) and 4.33 eV (2.69 %), respectively], while RevSCAN predicts a low Φ of 4.18 eV, giving the largest difference (6.06 %).

Table 7: The work function (eV) of Cu as calculated with each exchange-correlation DF, presented alongside previous computational and experimental results. Results from the current work are highlighted in bold, and the percentage difference (%) are given in parentheses relative to the experimental measurement of Rowe et al. [65] for the (111) facet, Gartland et al.[66] for the (100) facet, and Derry et al. [62] for the (110) facet.

DF \ Facet	(111)	(100)	(110)
PBE	**4.72** *(-4.45)*	**4.44** *(-3.27)*	**4.35** *(-2.25)*
Patra *et al.*[15]	4.78	4.42	4.38
Tran *et al.* [11]	4.88	4.47	4.19
Wang *et al* [67]	4.71	4.50	4.27
PBE+TS	**4.76** *(-3.64)*	**4.50** *(-1.96)*	**4.28** *(-3.82)*
PBE+MBD-NL	**4.71** *(-4.66)*	**4.45** *(-3.05)*	**4.23** *(-4.94)*
TPSS	**4.75** *(-3.85)*	**4.59** *(0.00)*	**4.50** *(+1.12)*
SCAN	**4.89** *(-1.01)*	**4.55** *(-0.87)*	**4.30** *(-3.37)*
Patra *et al.*[15]	4.98	4.43	4.48
revSCAN	**4.85** *(-1.82)*	**4.52** *(-1.52)*	**4.18** *(-6.06)*
mBEEF	**4.83** *(-2.23)*	**4.53** *(-1.31)*	**4.33** *(-2.69)*
Rowe *et al.* [65]	4.94 ± 0.03	-	-
Gartland *et al.* [66]	-	4.59 ± 0.03	-
Derry *et al.*[62]	-	-	4.45

For Zn, the work functions of the (0001) and (10-10) surface facets are given in Table 8. mBEEF provides the closest agreement with experiment for the (0001) facet, with a difference of 0.72 %, while PBE+TS gives the largest difference (-6.02 %). An experimental work function for the (10-10) facet is unavailable for comparison with the computed values; however, it is interesting to note for

the computed results that the work function is greater for this facet than the more stable (0001) facet, which is in contrast to the FCC metals, where the less stable surfaces have smaller work functions.

Table 8: The work function (eV) of Zn as calculated with each exchange-correlation DF, presented alongside previous computational and experimental results. Results from the current work are highlighted in bold, and the percentage difference (%) relative to the experimental measurement of Lang et al. [68] for the (0001) facet is also given for each facet in parentheses.

DF \ Facet	(0001)	(10-10)
PBE Tran *et al.*[11]	**3.96** *(-4.57)* 3.91	**4.35** 4.07
PBE+TS	**3.90** *(-6.02)*	**4.34**
PBE+MBD-NL	**3.91** *(-5.78)*	**4.31**
TPSS	**3.95** *(-4.82)*	**4.11**
SCAN	**4.00** *(-3.61)*	**4.10**
revSCAN	**4.35** *(-4.82)*	**4.68**
mBEEF	**4.18** *(+0.72)*	**4.49**
Lang *et al*.[69]	4.15	

Figure 5 summarises the observations in this section, presenting the percentage differences between calculated and experimental work functions for each element with each DF. All DFs have provided errors below 7 % for the three elements. As discussed, PBE gives the best agreement for Pd; TPSS and SCAN give the best agreement for Cu; and mBEEF gives the best agreement for Zn. A mean MPAE (i.e. mean of means) with respect to experiment has been proposed for the three considered elements: for this metric, mBEEF gives the lowest average difference of 1.94 %.

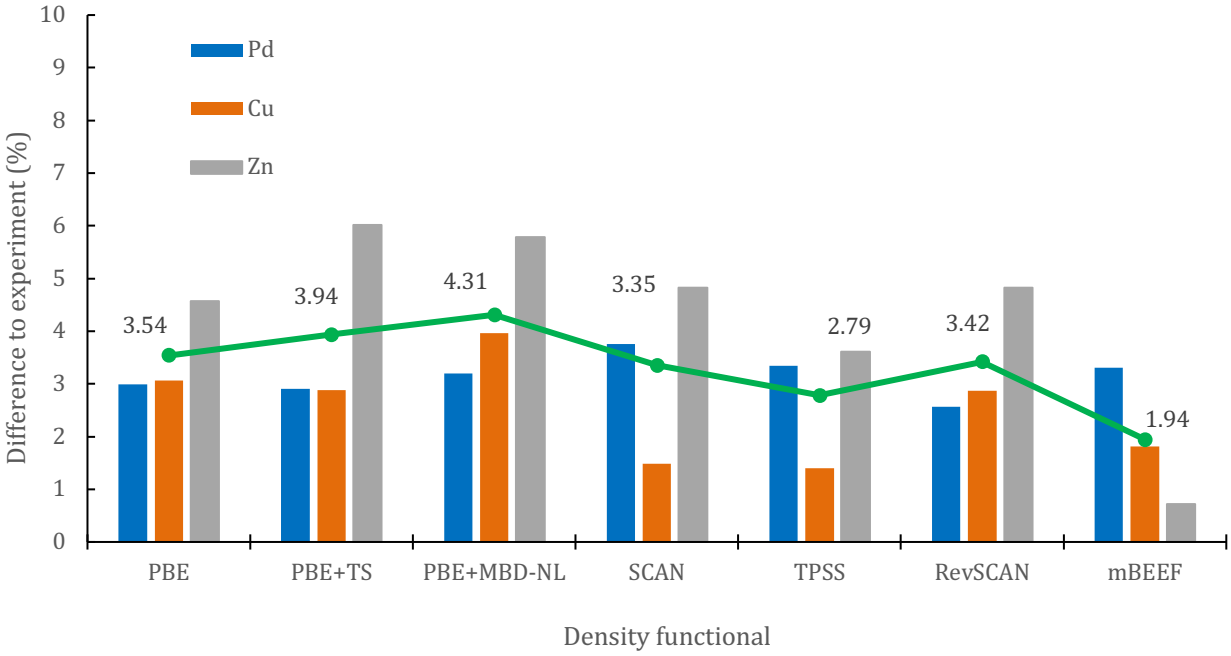

Figure 5: MPAE for the surface energy and work functions calculated for each element (Pd: Blue; Cu: Orange; Zn: Grey) with each DF, and the mean of these element specific MPAE (Green) for the different XC DFs.

Discussion

For the bulk lattice parameters and cohesive energies, seven DFs provide an MPAE below 6 % (PBE, PBE+TS, PBE+MBD-NL, TPSS, SCAN, revSCAN, mBEEF). These seven DFs were then applied in calculations of the energetics and electronic structure of material surfaces, with agreement against experiment varying for each element (Pd, Cu and Zn) when the DFs are compared. To draw together the observations and identify the best performing DFs, we summarise the key results here.

For bulk materials, mBEEF and PBE+MBD-NL provide the lowest differences relative to experiment, of 2.55 and 2.78 % in the MPAE respectively; when considering surface energies, the differences between computation and experiment are on average larger, and the DFs that performed well for bulk were worse performing: mBEEF (and PBE) generally underestimate the surface energies, while PBE+MBD-NL (revSCAN, and PBE+TS) overestimate. As well as the absolute energies being a metric of accuracy, one can also consider the relative surface energies as representing accurately the energetic ordering of surfaces for a given element: considering the ratio of the (111)/(100) surface energies for Pd, and comparing to the experimental results of Chen *et al.* [59], PBE and mBEEF are noted as agreeing better with experiment, with all other DFs giving values closer to unity.

For electronic work functions, SCAN and TPSS give (similar) results with good agreement to experiment for the Pd (111) and (100) facets, with SCAN also performing well for the Cu (111) facet and TPSS best performing for the Cu (100) and Cu (110) facet. For the other Pd facet, (110), mBEEF performs well, and similarly is closest to experiment for the Zn work function. When we average the deviations in calculated work functions from experiment, across all the density functionals, as shown in Figure 5, it is clear that mBEEF provides the lowest mean error. Overall, therefore, we highlight mBEEF as the most accurate options for general application to the different metals considered, and potentially therefore for more complex systems such as alloys.

Wulff construction

To conclude the current study and demonstrate the importance of DF choice when making assumptions of chemical reactivity for surfaces, we use surface energies obtained with the mBEEF DF to calculate optimal nanoparticle morphologies for systems with 5,000 atoms (Radius: 11 nm); morphologies obtained with PBE data are also shown for comparison. The relative stability of surface facets, and their intersection to form valid nanocrystal morphologies, is crucial for prediction of nanoparticle structures, with consequences in optical, medical and catalytic applications [70,71].

In order to ensure accuracy for the Wulff construction process, additional high index (332), (322), (211) and (221) facets were cleaved from the crystal bulk for Pd and Cu, and the stabilities evaluated; For Zn, Tran *et al.* [11] have shown that (0001) and (10-10) are significantly lower in energy than all other surfaces and so other high index facets were not considered here. Some high index surfaces offer comparable stability to the low index surface facets, and thus are observed in the outcomes of the Wulff construction. For Pd, the order of stability of all facets is (111) > (100)> (332) > (210) > (322); for Cu, a slight difference is noted with both the (111) and (100) facets more stable (i.e. lower in energy) than the (322) > (332) > (221) > (110) > (210) facets. The work functions were also calculated for the high index facets (SI, Table S4), and in general are inversely related to the surface energy for these FCC metals, though not strictly: the Pd and Cu (221) facets give the smallest value of Φ, with the (110) and (210) facets providing the next smallest values.

The structures predicted by the Wulff construction for a 5,000 atoms nanoparticle of Pd, Cu and Zn are given in Figure 6. The morphology predicted for all three species is in good agreement with other computational work by Tran *et al.* [11] and Lin *et al.* [57]. The surface coverage of each facet type, presented in Table 9, shows that the (111) facet is most prevalent for Pd (48.83 %), followed by the (100) facet (18.80 %). The high index (332) and (210) facets cover 18.30 % and 6.96 %, respectively. Whilst not the highest in surface energy, we note that the (110) facet is not present, in agreement with the Wulff construction provided by Tran *et al.* [11]

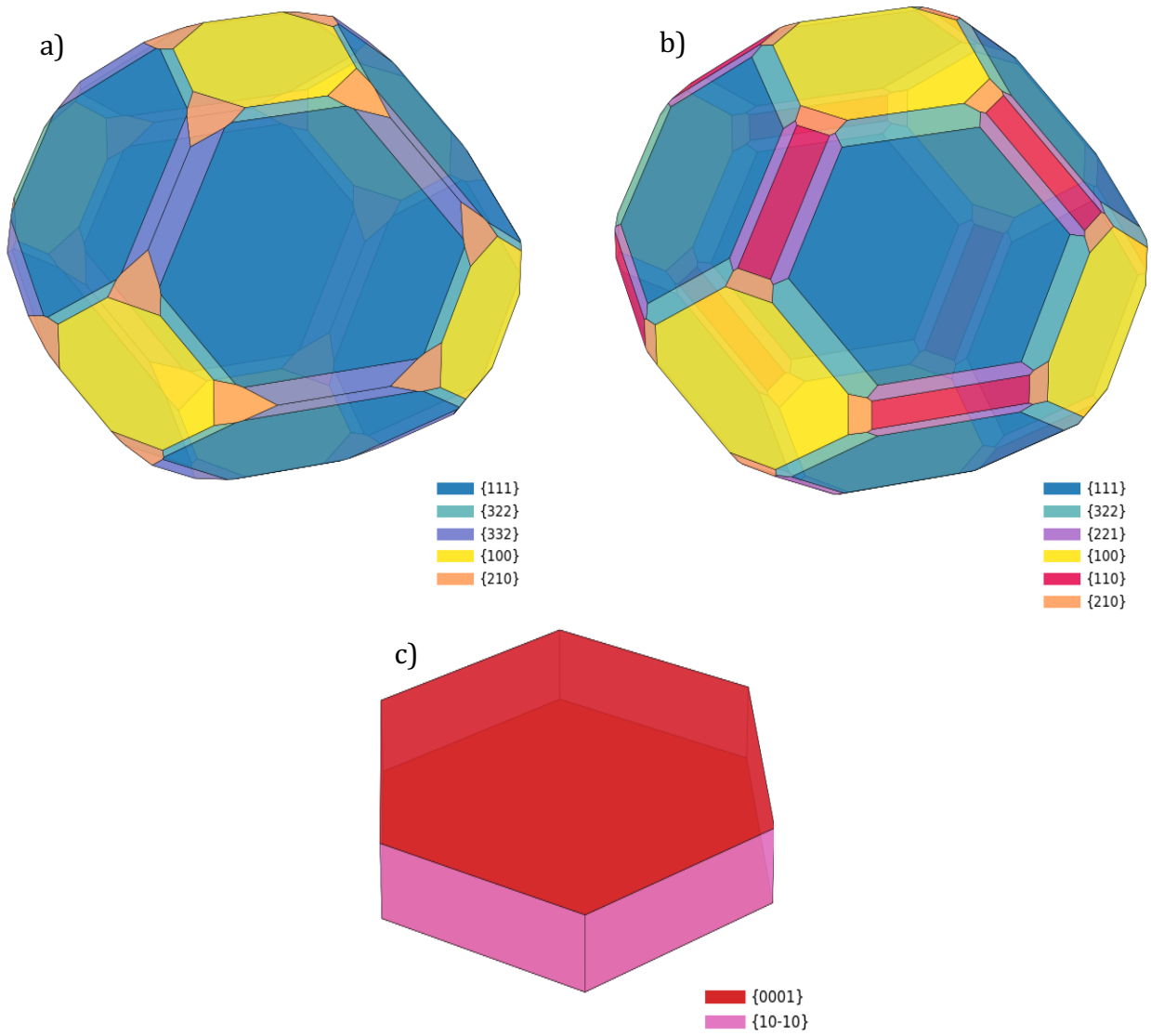

Figure 6: The crystal morphology calculated by Wulff construction for a) Pd, b) Cu and c) Zn nanoparticles of 5,000 atoms.

To provide a demonstration of the impact that DF choices have on nanoparticle structure, and the consequences for investigations of reactivity we also, as noted, computed the Wulff construction considering the surface energies calculated with the widely used PBE approach; the outcomes show that the Pd (100) facet has a 10 % higher surface coverage with mBEEF. The (210) facet was absent in the Wulff construction using mBEEF while it represents 1.26 % using PBE. Such information is critical in understanding the behaviour of Pd nanoparticles toward catalytic reaction: Zhang *et al.* [72] have compared the reactivity of (111) and (100) facets toward CO_2 reaction and concluded, by comparing the activation energies of the two facets, that the (100) is more reactive than the (111).

Having the (100) facet more abundant in the nanoparticle as obtained from the mBEEF Wulff construction would result in a more reactive nanoparticle. No experimental proof of the existence of (210) facet for Pd has been found in current literature.

Table 9: Surface energy (J/m^2) and surface coverage (%) for a nanoparticle with 5,000 atoms, obtained with the mBEEF DF, for Pd, Cu, and Zn . For comparison, values given in parentheses are results calculated with the PBE DF.

Facet	Surface energy	Surface coverage	Surface energy	Surface coverage
	Pd		Cu	
(111)	1.32 (1.36)	48.83 (48.81)	1.43 (1.37)	47.83 (57.32)
(100)	1.50 (1.54)	18.80 (9.29)	1.56 (1.51)	23.91 (25.84)
(110)	1.58 (1.60)	0.00 (0.00)	1.63 (1.58)	8.10 (6.97)
(332)	1.41 (1.45)	18.30 (19.59)	1.57 (1.50)	0.00 (0.00)
(322)	1.45 (1.50)	7.11 (4.19)	1.55 (1.51)	10.47 (0.02)
(221)	1.49 (1.51)	0.00 (1.26)	1.58 (1.53)	6.73 (6.72)
(210)	1.59 (1.63)	6.96 (7.53)	1.70 (1.66)	2.95 (2.94)
	Zn			
(0001)	0.24 (0.32)	71.02 (60.24)		
(10-10)	1.17 (0.97)	28.98 (39.75)		

For Cu, the most prominent facet is again the (111), with a descending order of surface coverage thus: (111) > (100) > (332) > (110) > (221) and (210). In contrast to Pd, the (322) facet was not observed. Tran *et al.*[11] obtained a similar result for the absence of the (322) facet, though did predict the presence of (331), (311) and (310) facets. Again, we computed a Wulff construction with the PBE DF for comparison and identify notable differences in the surface coverages when changing the DF: for mBEEF, the (111) surface coverage is 10 % lower than when using PBE, and for mBEEF the (322) facet has a 10% coverage whereas is essentially absent in the PBE model; such differences could be significant when designing nanocatalysts based on DFT calculations, thus demonstrating the impact of DF choice.

For Zn, a simple hexagonal closed packed morphology is formed by the two main (0001) and (10-10) facets, covering 71.02 % and 28.98 % of the surface, respectively, while with PBE this coverage is 64.24 % and 39.75 %, respectively. The Zn results are in close agreement with the TEM presented by Mai et al.[73], as well as the theoretical work of Tran et al.[11].

Summary and Conclusions

The impact of computational settings for density functional theory simulations of Pd, Cu and Zn materials have been investigated, considering both bulk and surface models. An initial set of 22 density functionals was considered and used to calculate the cohesive energy and lattice parameters for the optimized bulk unit cell of each element. The following density functionals provide relatively low mean percentage average errors (< 6 %) relative to experiment: PBE, PBE+TS, PBE+MBD-NL, TPSS, SCAN, revSCAN, and mBEEF.

The selected density functionals were further used to study low-index surfaces. To remove the presence of quantum size effects, a minimum model thickness of 7 atomic layers perpendicular to the surface plane were necessary, as well as a dense **k**-grid of one **k**-point per (0.018 x 2π) $Å^{-1}$. The surface energies obtained agree reasonably with experiment. It is noted that vdW corrections considered on PBE calculations, namely PBE+TS and PBE+MBD-NL, increase the surface energy of all three elements, with particularly poor outcomes for Cu surfaces with PBE+TS. By considering the computed absolute and relative surface energies, work functions, and previously highlighted bulk observables, and comparing to a range of experimental data, we can conclude that mBEEF offers the greatest accuracy of the bulk and surface properties of these metals. The significance of this conclusion is demonstrated by a comparison of nanoparticles formed using Wulff construction with mBEEF and PBE computed surface energies, showing surface coverage differences of some facets of up to 10 %. The conclusion provides a sound basis for the use of this density functional, together with the **k**-point and layer thickness settings discussed above, for future computational studies of these metals and their alloys.

Conflicts of Interest

There are no conflicts of interest to declare.

Acknowledgements

The authors are grateful for funding by the EPSRC Centre-to Centre Project (Grant reference: EP/S030468/1). We are grateful to Matthias Scheffler, Yuanyuan Zhou, Herzain Rivera, Graham Hutchings and David Willock for useful discussions. AJL acknowledges funding by the UKRI Future Leaders Fellowship program (MR/T018372/1). The authors acknowledge computational resources and support from: the Supercomputing Wales project, which is part-funded by the European Regional Development Fund (ERDF) via the Welsh Government; the UK National Supercomputing Service YOUNG, accessed via membership of the Materials Chemistry Consortium which is funded by Engineering and Physical Sciences Research Council (EP/L000202/1, EP/R029431/1, EP/T022213/1); and the Isambard UK National Tier-2 HPC Service operated by GW4 and the UK Met Office, and funded by EPSRC (EP/P020224/1).

References

1. Tavares, S. R. *et al.* DFT calculations for structural prediction and applications of intercalated lamellar compounds. *Dalt. Trans.* **47**, 2852–2866 (2018).
2. Da Silva, J. L. F., Stampfl, C. & Scheffler, M. Converged properties of clean metal surfaces by all-electron first-principles calculations. *Surf. Sci.* **600**, 703–715 (2006).
3. Miller, W. & Tyson, W. Surface free energies of solid metals. Estimation from liquid surface tension measurements. *Surf. Sci.* **62**, 267–276 (1977).
4. Gilman, J. J. Direct measurements of the surface energies of crystals. *J. Appl. Phys.* **31**, 2208–2218 (1960).
5. Eaglesham, D. J., White, A. E., Feldman, L. C, Moriya, N. & Jacobson, D. C. Equilibrium shape of Si. *Phys. Rev. Lett.* **70**, 1643–1646 (1993).
6. G. Lang. Surface Tension of Llquid Elements,. **54th ed**, 7–19.
7. M. Methfessel, D. Henning, M. S. Trends of the surface relaxations, surface energies, and work functions of the 41 transition metals. *Phys. Rev. B 46* **46**, 4816–4829 (1992).
8. J. Kollár, L. Vitos, H. L. S. ,. *Phys. Rev. B* **49**, 11288 (1994).
9. Vitos, L., Ruban, A. V, Skriver, H. L. & Kolla, J. The surface energy of metals. *Surf. energy Met.* **411**, 186–202 (1998).
10. Zhang, X., Yang, W. & Dong, C. Levoglucosan formation mechanisms during cellulose pyrolysis. *J. Anal. Appl. Pyrolysis* **104**, 19–27 (2013).
11. Tran, R., Xu, Z., Radhakrishnan, B., Winston, D. & Sun, W. Data Descriptor : Surface energies of elemental crystals. *Sci. Data* **3**, 1–13 (2016).
12. Rodriguez, A. M., Bozzolo, G. & Ferrante, J. Multilayer relaxation and surface energies of fee and bee metals using equivalent crystal theory. **289**, (1993).
13. Cramer, C. J. & Truhlar, D. G. Density functional theory for transition metals and transition metal chemistry. *Phys. Chem. Chem. Phys.* **11**, 10757–10816 (2009).

14. Perdew, J. P., Burke, K. & Ernzerhof, M. Generalized gradient approximation made simple. *Phys. Rev. Lett.* **77**, 3865–3868 (1996).

15. Patra, A., Bates, J. E., Sun, J. & Perdew, J. P. Properties of real metallic surfaces: Effects of density functional semilocality and van der Waals nonlocality. *Proc. Natl. Acad. Sci. U. S. A.* **114**, E9188–E9196 (2017).

16. Sabatini, Riccardo and Gorni, Tommaso and de Gironcoli, S. Nonlocal van der Waals density functional made simple and efficient. *Phys. Rev. B* **87**, 041108(1–4) (2013).

17. Zeng, X. M., Huang, R., Shao, G. F., Wen, Y. H. & Sun, S. G. High-index-faceted platinum nanoparticles: Insights into structural and thermal stabilities and shape evolution from atomistic simulations. *J. Mater. Chem. A* **2**, 11480–11489 (2014).

18. S.L. Bernasek, G. A. S. Small molecule reactions on stepped single crystal platinum surfaces. *Surf. Sci.* **48**, 204–213 (1975).

19. Tian, N., Zhou, Z. Y. & Sun, S. G. Platinum metal catalysts of high-index surfaces: from single-crystal planes to electrochemically shape-controlled nanoparticles. *J. Phys. Chem. C* **112**, 19801–19817 (2008).

20. Quan, Z., Wang, Y. & Fang, J. High-Index Faceted Noble Metal Nanocrystals. *Acc. Chem. Res.* **46**, 191–202 (2013).

21. Jin, M., Zhang, H., Xie, Z. & Xia, Y. Palladium concave nanocubes with high-index facets and their enhanced catalytic properties. *Angew. Chemie - Int. Ed.* **50**, 7850–7854 (2011).

22. V. Blum, R. Gehrke, F. Hanke, P. Havu, V.Havu, X. Ren, K. Reuter, M. S. The Fritz Haber Institute ab initiomolecular simulations package (FHI-aims). (2009).

23. Lehtola, S., Steigemann, C., Oliveira, M. J. T. & Marques, M. A. L. Recent developments in LIBXC — A comprehensive library of functionals for density functional theory. *SoftwareX* **7**, 1–5 (2018).

24. Huhn, William P. and Blum, V. One-hundred-three compound band-structure benchmark of

post-self-consistent spin-orbit coupling treatments in density functional theory. *Phys. Rev. Mater.* **1**, 033803–033821 (2017).

25. Tkatchenko, A. & Scheffler, M. Accurate molecular van der Waals interactions from ground-state electron density and free-atom reference data. *Phys. Rev. Lett.* **102**, 6–9 (2009).

26. Hermann, J. & Tkatchenko, A. Density Functional Model for van der Waals Interactions: Unifying Many-Body Atomic Approaches with Nonlocal Functionals. *Phys. Rev. Lett.* **124**, 1–7 (2020).

27. NJ.P. Perdew, A. Ruzsinszky, G.I. Csonka, O.A. Vydrov, G.E. Scuseria, L.A. Constantin, X. Zhou, and K. B. NJ.P. Perdew, A. Ruzsinszky, G.I. Csonka, O.A. Vydrov, G.E. Scuseria, L.A. Constantin, X. Zhou, and K. Burke. Phys. Rev. Lett., 100:136406, 2008. o Title. *Phys. Rev. Lett* **100**, 100:136406 (2008).

28. Zhang, Y. & Yang, W. Comment on "generalized gradient approximation made simple". *Phys. Rev. Lett.* **80**, 890 (1998).

29. Hammer, B., Hansen, L. B. & Nørskov, J. K. Improved adsorption energetics within density-functional theory using revised Perdew-Burke-Ernzerhof functionals. *Phys. Rev. B - Condens. Matter Mater. Phys.* **59**, 7413–7421 (1999).

30. Fabiano, E., Constantin, L. A. & Della Sala, F. Generalized gradient approximation bridging the rapidly and slowly varying density regimes: A PBE-like functional for hybrid interfaces. *Phys. Rev. B - Condens. Matter Mater. Phys.* **82**, 1–4 (2010).

31. Vydrov, O. A. & Van Voorhis, T. Nonlocal van der Waals density functional: The simpler the better. *J. Chem. Phys.* **133**, (2010).

32. Grimme S. Semiempirical GGA-Type Density Functional Constructed with a Long-Range Dispersion Correction. *J Comput Chem* **27**, 1787–1799 (2006).

33. Nattino, Francesco and Díaz, Cristina and Jackson, Bret and Kroes, G.-J. Effect of Surface Motion on the Rotational Quadrupole Alignment Parameter of D_2 Reacting on Cu(111). *Phys.*

Rev. Lett. **108**, 236104 (2012).

34. Boese, A. D. & Handy, N. C. A new parametrization of exchange-correlation generalized gradient approximation functionals. *J. Chem. Phys.* **114**, 5497–5503 (2001).

35. Lee, Chengteh and Yang, Weitao and Parr, R. G. Development of the Colle-Salvetti correlation-energy formula into a functional of the electron density. *Phys. Rev. B* **37**, 785–789 (1988).

36. Sun, J., Ruzsinszky, A. & Perdew, J. Strongly Constrained and Appropriately Normed Semilocal Density Functional. *Phys. Rev. Lett.* **115**, 1–6 (2015).

37. Mezei, P. D., Csonka, G. I. & Kállay, M. Simple Modifications of the SCAN Meta-Generalized Gradient Approximation Functional. *J. Chem. Theory Comput.* **14**, 2469–2479 (2018).

38. Tao, Jianmin and Perdew, John P. and Staroverov, Viktor N. and Scuseria, G. E. Climbing the Density Functional Ladder: Nonempirical Meta--Generalized Gradient Approximation Designed for Molecules and Solids. *Phys. Rev. Lett.* **91**, 146401 (2003).

39. Constantin, Lucian and Fabiano, Eduardo and Della Sala, F. Semilocal dynamical correlation with increased localization. *Phys. Rev. B* **86**, 035130 (2012).

40. Garza, A. J., Bell, A. T. & Head-Gordon, M. Nonempirical Meta-Generalized Gradient Approximations for Modeling Chemisorption at Metal Surfaces. *J. Chem. Theory Comput.* **14**, 3083–3090 (2018).

41. Wellendorff, J., Lundgaard, K. T., Jacobsen, K. W. & Bligaard, T. MBEEF: An accurate semi-local Bayesian error estimation density functional. *J. Chem. Phys.* **140**, (2014).

42. Adamo, C. & Barone, V. Toward reliable density functional methods without adjustable parameters: The PBE0 model. *J. Chem. Phys.* **110**, 6158–6170 (1999).

43. Stephens, P. J., Devlin, F. J., Chabalowski, C. F. & Frisch, M. J. Ab Initio calculation of vibrational absorption and circular dichroism spectra using density functional force fields. *J.*

Phys. Chem. **98**, 11623–11627 (1994).

44. Heyd, J., Scuseria, G. E. & Ernzerhof, M. Hybrid functionals based on a screened Coulomb potential. *J. Chem. Phys.* **118**, 8207–8215 (2003).

45. Hebbache, M. & Zemzemi, M. Ab initio study of high-pressure behavior of a low compressibility metal and a hard material: Osmium and diamond. *Phys. Rev. B - Condens. Matter Mater. Phys.* **70**, 5–10 (2004).

46. Hjorth Larsen, A. *et al.* The atomic simulation environment - A Python library for working with atoms. *J. Phys. Condens. Matter* **29**, (2017).

47. Nocedal J. & Wright S. J. *Numerical Optimization*. *Springer Series in Operations Research and Financial Engineering* vol. 83 (springer, 2006).

48. Broqvist, P., Grönbeck, H. & Panas, I. Surface properties of alkaline earth metal oxides. *Surf. Sci.* **554**, 262–271 (2004).

49. Singh-Miller, Nicholas E. and Marzari, N. Surface energies, work functions, and surface relaxations of low-index metallic surfaces from first principles. *Phys. Rev. B* **80**, 235407 (2009).

50. Gao, L., Souto-Casares, J., Chelikowsky, J. R. & Demkov, A. A. Orientation dependence of the work function for metal nanocrystals. *J. Chem. Phys.* **147**, (2017).

51. Rahm, J. & Erhart, P. WulffPack: A Python package for Wulff constructions. *J. Open Source Softw.* **5**, 1944 (2020).

52. Gražulis S, Chateigner D, Downs RT, Yokochi AF, Quirós M, Lutterotti L, Manakova E, Butkus J, Moeck P, L. B. A. Crystallography Open Database - an open-access collection of crystal structures. *J Appl Crystallogr.* **42**, 726–729 (2009).

53. Lejaeghere, K., Van Speybroeck, V., Van Oost, G. & Cottenier, S. Error estimates for solid-state density-functional theory predictions: An overview by means of the ground-state elemental crystals. *Crit. Rev. Solid State Mater. Sci.* **39**, 1–24 (2014).

54. Janthon, P. *et al.* Bulk properties of transition metals: A challenge for the design of universal density functionals. *J. Chem. Theory Comput.* **10**, 3832–3839 (2014).

55. Schulte, F. K. A theory of thin metal films: electron density, potentials and work function. *Surf. Sci.*, **55**, 427–444 (1976).

56. Pandey, S. K., Das, R. & Mahadevan, P. Layer-Dependent Electronic Structure Changes in Transition Metal Dichalcogenides: The Microscopic Origin. *ACS Omega* **5**, 15169–15176 (2020).

57. Lin, H., Lin, H., Liu, J. X., Fan, H. & Li, W. X. Compensation between Surface Energy and hcp/fcc Phase Energy of Late Transition Metals from First-Principles Calculations. *J. Phys. Chem. C* **124**, 11005–11014 (2020).

58. Tyson, W. R. Surface energies of solid metals. *Can. Metall. Q.* **14**, 307–314 (1975).

59. Chen, P., Gao, Y. & Castell, M. R. Experimental determination of the {111}/{001} surface energy ratio for Pd crystals. *Appl. Phys. Lett.* **117**, 1–5 (2020).

60. Da Silva, J. L. F., Barreteau, C., Schroeder, K. & Blügel, S. All-electron first-principles investigations of the energetics of vicinal Cu surfaces. *Phys. Rev. B - Condens. Matter Mater. Phys.* **73**, 1–11 (2006).

61. Fischer, R. *et al.* Image States and Local Work Function for Ag/Pd(lll). *Phys. Rev. Lett.* 6–9 (1993).

62. Derry, G. N., Kern, M. E. & Worth, E. H. Recommended values of clean metal surface work functions. *J. Vac. Sci. Technol. A Vacuum, Surfaces, Film.* **33**, 060801 (2015).

63. Bordoloi, A. K. & Auluck, S. Electronic structure of palladium. *Phys. Rev. B* **27**, 5116–5118 (1983).

64. Sesselmann, W., Woratschek, B., Küppers, J., Ertl, G. & Haberland, H. Interaction of metastable noble-gas atoms with transition-metal surfaces: Resonance ionization and Auger neutralization. *Phys. Rev. B* **35**, 1547–1559 (1987).

65. Rowe, J. E., Smith, N. V. Photoemission spectra and band structures of d-band metals. V. The (100) and (111) faces of single-crystal copper. *Phys. Rev. B* **10**, 3207–3212 (1974).

66. Gartland, P. O., Berge, S. & Slagsvold, B. J. Photoelectric Work Function of a Copper Single Crystal. **28**, (1972).

67. Wang, J. & Wang, S. Q. Surface energy and work function of fcc and bcc crystals: Density functional study. *Surf. Sci.* **630**, 216–224 (2014).

68. Lang, N. D. & Kohn, W. Theory of metal surfaces: Work function. *Phys. Rev. B* **3**, 1215–1223 (1971).

69. Akbi, M. & Lefort, A. Work function measurements of contact materials for industrial use. *J. Phys. D. Appl. Phys.* **31**, 1301–1308 (1998).

70. Pihlajamäki, A. *et al.* Monte Carlo Simulations of Au38(SCH3)24 Nanocluster Using Distance-Based Machine Learning Methods. *J. Phys. Chem. A* **124**, 4827–4836 (2020).

71. McNamara, K. & Tofail, S. A. M. Nanoparticles in biomedical applications. *Adv. Phys. X* **2**, 54–88 (2017).

72. Zhang, C. J. & Hu, P. CO oxidation on Pd(100) and Pd(111): A comparative study of reaction pathways and reactivity at low and medium coverages. *J. Am. Chem. Soc.* **123**, 1166–1172 (2001).

73. Banyasz, J. L., Li, S., Lyons-Hart, J. L. & Shafer, K. H. Cellulose pyrolysis: The kinetics of hydroxyacetaldehyde evolution. *J. Anal. Appl. Pyrolysis* **57**, 223–248 (2001).